JACS
JOURNAL OF THE AMERICAN CHEMICAL SOCIETY

Article

pubs.acs.org/JACS

Rectifying Electron-Transport Properties through Stacks of Aromatic Molecules Inserted into a Self-Assembled Cage

Shintaro Fujii,*[,†] Tomofumi Tada,*[,‡] Yuki Komoto,[†] Takafumi Osuga,[§] Takashi Murase,[∥] Makoto Fujita,*[,§] and Manabu Kiguchi*[,†]

[†]Department of Chemistry, Graduate School of Science and Engineering, Tokyo Institute of Technology, 2-12-1 W4-10 Ookayama, Meguro-ku, Tokyo 152-8511, Japan

[‡]Materials Research Center for Element Strategy, Tokyo Institute of Technology, 4259-S2-13 Nagatsuta-cho, Midori-ku, Yokohama 226-8503, Japan

[§]Department of Applied Chemistry, School of Engineering, The University of Tokyo, 7-3-1 Hongo, Bunkyo-ku, Tokyo 113-8656, Japan

[∥]Department of Material and Biological Chemistry, Faculty of Science, Yamagata University, 1-4-12 Kojirakawa-machi, Yamagata-shi, Yamagata 990-8560, Japan

Supporting Information

ABSTRACT: Aromatic stacks formed through self-assembly are promising building blocks for the construction of molecular electronic devices with adjustable electronic functions, in which noncovalently bound π-stacks act as replaceable modular components. Here we describe the electron-transport properties of single-molecule aromatic stacks aligned in a self-assembled cage, using scanning probe microscopic and break junction methods. Same and different modular aromatic pairs are noncovalently bound and stacked within the molecular cage holder, which leads to diverse electronic functions. The insertion of same pairs induces high electronic conductivity (10^{-3}–10^{-2} G_0, $G_0 = 2e^2/h$), while different pairs develop additional electronic rectification properties. The rectification ratio was, respectively, estimated to be 1.4–2 and >10 in current–voltage characteristics and molecular orientation-dependent conductance measurements at a fixed bias voltage. Theoretical calculations demonstrate that this rectification behavior originates from the distinct stacking order of the internal aromatic components against the electron-transport direction and the corresponding lowest unoccupied molecular orbital conduction channels localized on one side of the molecular junctions.

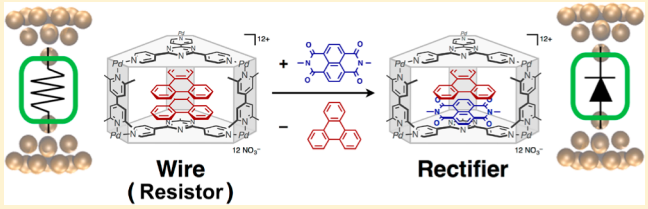

INTRODUCTION

The ability to understand and control charge transport properties on the single-molecule scale has been a long-standing issue toward the realization of nanoscale electronic devices where individual molecules or molecular complexes act as electronic components. To functionalize electron transport properties at the single-molecule level, the individual component molecules must be precisely aligned in place and function adequately in nanometer-scale devices.[1,2] The mechanically controllable break junction (MCBJ) technique[3−6] has made it possible to reveal the electron transport properties of single-molecule junctions[7−11] as molecular switches,[12−20] diodes,[21−25] and transistors,[26−31] in which the component molecules are covalently connected, and therefore the entire electronic functionality is invariable. One promising method to add flexible functional tunability is to integrate host–guest systems into the molecular junction,[32,33] where the electronic functionality can be, in principle, flexibly tuned by the insertion of guest molecules.

Columnar self-assembled cage **1** accommodates planar aromatics in the box-shaped cavity to provide discrete π-stacked systems in solution (Figure 1). The stacking number of accommodated aromatics is uniquely dictated by the cage height (i.e., two aromatics in cage **1**).[34] In addition to the stacking number, cage **1** also controls the stacking pair of accommodated aromatics when two different aromatics are employed.[35] For example, naphthalenediimide (**2**, electron acceptor) and triphenylene (**3**, electron donor) are selectively paired and strongly bound within the cage, which results in the quantitative formation of thermodynamically stable ternary complex **1**·(**2**·**3**). As a result, the hetero π-stacked complex **1**·(**2**·**3**) is more stable than the homo π-stacked complexes **1**·(**2**·**2**) and **1**·(**3**·**3**), and the site-exchange between **2** and **3** in the heterocomplex does not occur at room temperature on the nuclear magnetic resonance time scale. Hence, cage **1** serves as a molecular holder to precisely align aromatics in place and to modulate electron-transport properties at the single-molecule level.[32,33]

Received: January 5, 2015
Published: April 21, 2015

DOI: 10.1021/jacs.5b00086
J. Am. Chem. Soc. 2015, 137, 5939–5947

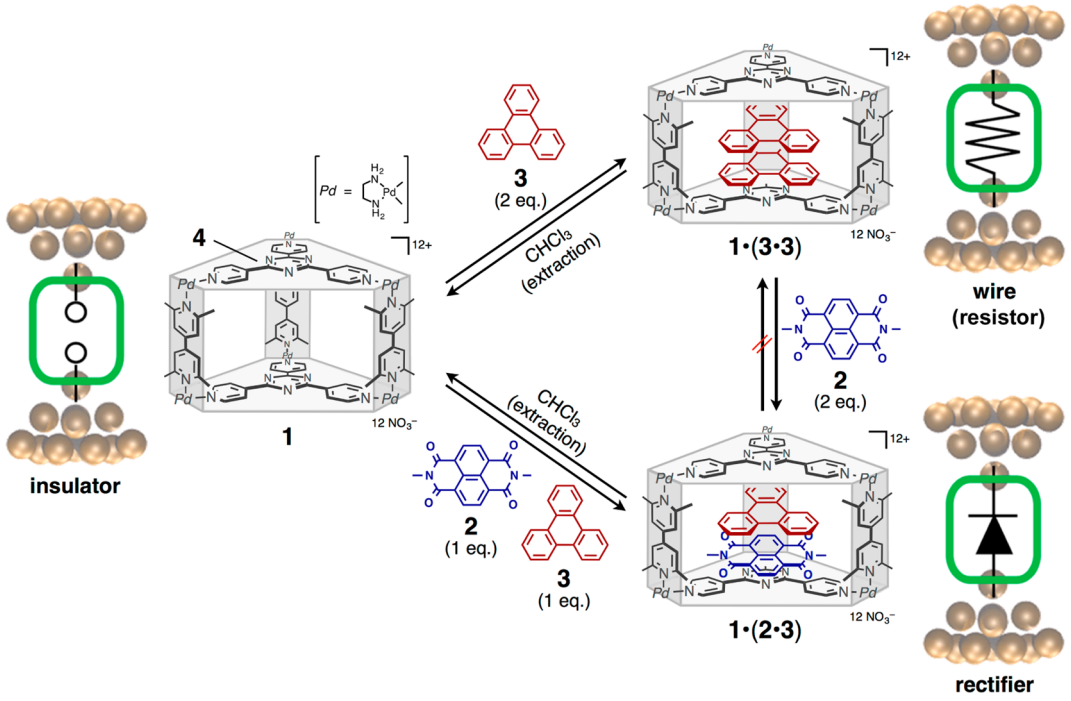

Figure 1. Schematic representation of single-molecule junctions sandwiched by two Au electrodes and the corresponding electronic components of the junctions. Columnar cage **1** can accommodate a pair of naphthalenediimide (**2**) and triphenylene (**3**) or a dimer of **3**, in which the enclosed aromatic pair is bookended by the electron-poor triazine panels **4** of the cage. Empty cage **1**, homo π-stacked complex **1**·(**3**·**3**), and hetero π-stacked complex **1**·(**2**·**3**) behave as close as an insulator, a wire (resistor), and a rectifier, respectively. Heterocomplex **1**·(**2**·**3**) is more stable than homocomplexes **1**·(**2**·**2**) and **1**·(**3**·**3**). Although homocomplex **1**·(**3**·**3**) is quantitatively formed, homocomplex **1**·(**2**·**2**) is obtained[35] at very low yield and is therefore not discussed in this study.

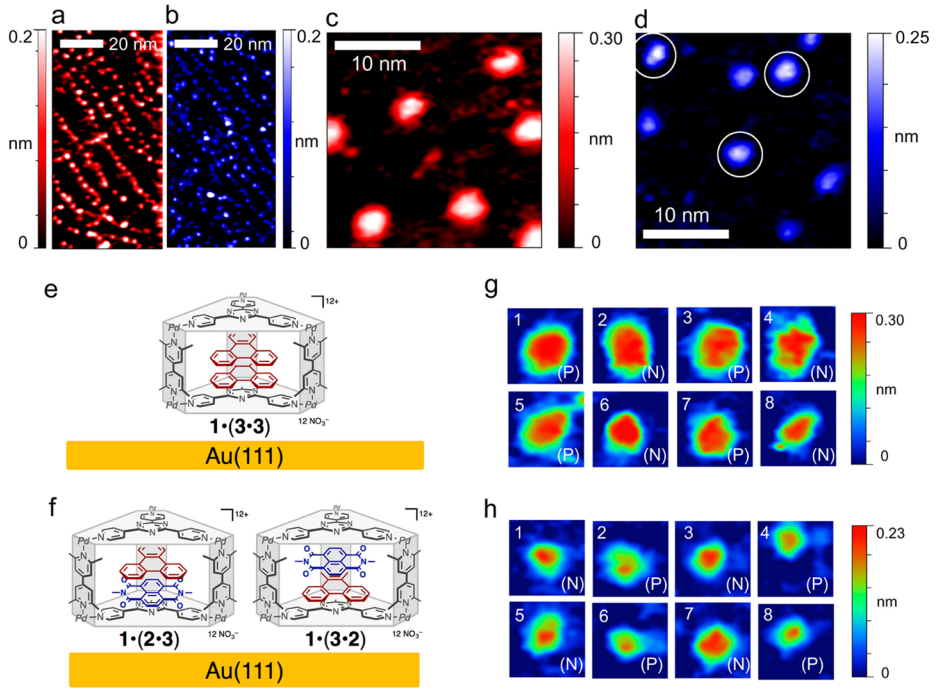

Figure 2. Individual π-stacked molecules on Au(111) surface. (a,b) Large scale STM images of (a) homocomplex **1**·(**3**·**3**) and (b) heterocomplex **1**·(**2**·**3**) on a Au(111) surface under ambient conditions at room temperature (imaging area = 50 × 100 nm^2, tunneling current (I_t) = 100 pA, sample bias voltage (V_s) = 1.0 V). (c,d) Magnified STM images of homocomplex **1**·(**3**·**3**) (c) and heterocomplex **1**·(**2**·**3**) (d) on Au(111) surfaces (imaging area = 25 × 25 nm^2, I_t = 200 pA, V_s = 0.5 V). Circles in (d) indicate brighter and more conductive images than others. (e,f) Schematic illustration of typical adsorption structures of (e) homocomplex **1**·(**3**·**3**) and (f) heterocomplex **1**·(**2**·**3**) on Au(111) surfaces. Note that the stacking orders of **2**·**3** and **3**·**2** within cage **1** on the Au surface are distinctly different. (g,h) Bias voltage dependence of the STM images for the isolated (g) homo and (h) hetero complexes on Au(111) surfaces (imaging area = 6 × 6 and 5 × 5 nm^2 for homo and hetero complexes, respectively). The number at the upper left corner denotes the imaging order. The sample bias polarity is indicated by (P): +0.5 V or (N): −0.5 V at the bottom right corner in each image.

DOI: 10.1021/jacs.5b00086
J. Am. Chem. Soc. 2015, 137, 5939−5947

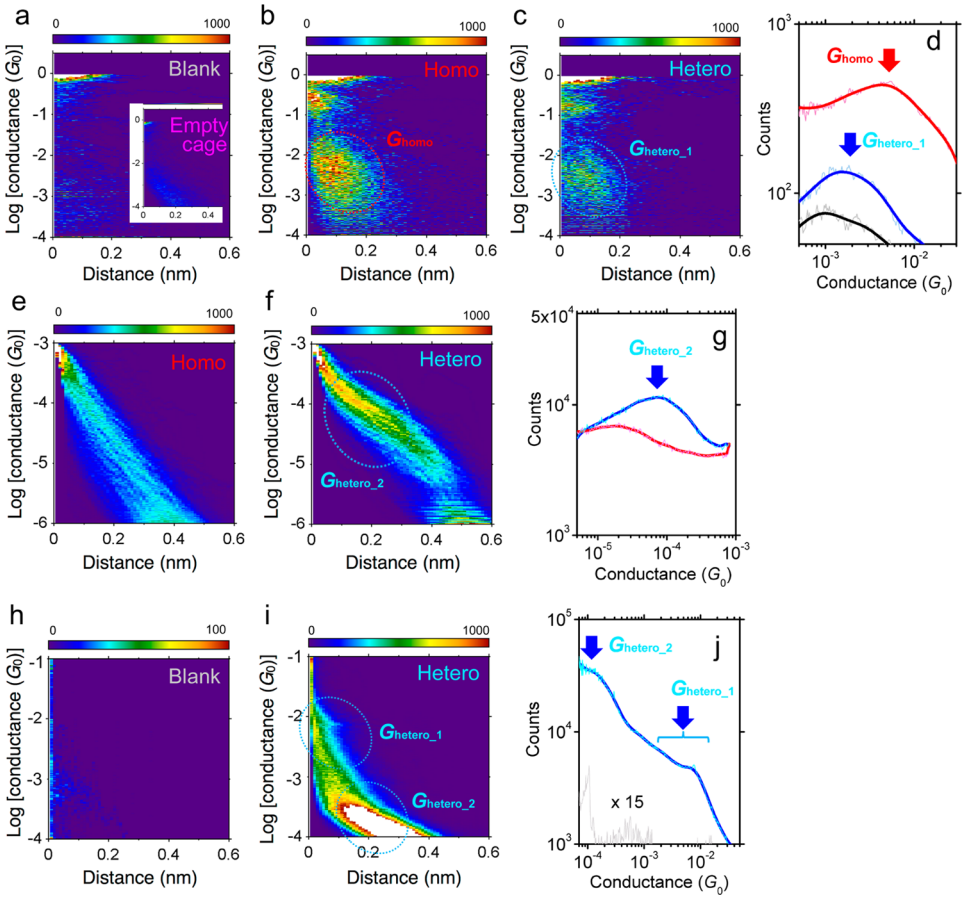

Figure 3. (a–c) 2D conductance-trace histograms for (a) blank and (b,c) π-stacked complexes sandwiched between Au electrodes in under liquid environment. The inset in (a) shows a 2D histogram for empty cage **1**, where no preferential conductance is apparent in the conductance range below 1 G_0. (For further details, see Supporting Information 2.) (b,c) Preferential intensities of G_{homo} and G_{hetero_1} are marked by dotted circles for homocomplex **1**·(**3**·**3**) and heterocomplex **1**·(**2**·**3**). Throughout this paper a linear bin-size of 0.01 nm and a logarithmic Y-bin-size for $\Delta\log(G/G_0)$ of 0.01 were used for construction of 2D conductance-trace histograms. (d) 1D Conductance histograms for blank (black), homocomplex (red) and heterocomplex (blue) where conductance peaks are denoted by arrows of G_{homo} and G_{hetero_1}. Bold lines are averaged and smoothed data. (a–d) The histograms were constructed from 2200 traces at a bias voltage of 20 mV. Unless otherwise noted a logarithmic bin-size for $\Delta\log(G/G_0)$ of 0.01 were used for 1D conductance histograms. (e,f) 2D histograms for molecular junctions of (e) homocomplex and (f) heterocomplex fabricated under ultrahigh vacuum (UHV) conditions, where preferential conductance of G_{hetero_2} is marked by a dotted circle in (f). (g) 1D Conductance histograms for homocomplex (red) and heterocomplex (blue) where a conductance peak is indicated by an arrow of G_{hetero_2}. The histograms of (e,f) were constructed from 1000 traces at a bias voltage of 150 mV. (h,i) 2D histograms for (h) blank and molecular junctions of (i) heterocomplex measured under UHV conditions. (h–j) The histograms of were constructed from 2000 traces at a bias voltage of 100 mV. Conductance peaks are indicated by arrows. Counts are multiplies by a factor of 15 for blank.

Herein, we describe the electron conductivity of the molecular holders containing modular aromatics, i.e., homocomplex **1**·(**3**·**3**) and heterocomplex **1**·(**2**·**3**), fixed between two Au electrodes, using scanning tunneling microscopy (STM) and the STM-break junction (STM-BJ) technique. The component aromatics are noncovalently embedded in the cage, and therefore, the entire electronic functionality can be modulated by replacing the aromatics with others (Figure 1). While the empty cage **1** exhibits insulating characteristics (ca. 10^{-5} G_0),[32] $G_0 = 2e^2/h$, see also Supporting Information 2), the insertion of modular aromatics **2** and/or **3** makes the cage highly conductive. For example, homocomplex **1**·(**3**·**3**) is several orders of magnitude more conductive (ca. 10^{-3}–10^{-2} G_0) than empty cage **1**, which ensures that electron transport is exclusively conducted through the inner aligned π-stacked aromatics. More importantly, replacement of the modular aromatic in the cage induces additional electronic functions, so that the heterocomplex **1**·(**2**·**3**) exhibits two distinct conductance states, which indicates the development of rectification properties that originate from the different stacking order, **2**·**3** or **3**·**2**, in the junction configuration, against the electron-transport direction. Therefore, even though π-acceptor **2** and π-donor **3** are not covalently connected with each other, heterocomplex **1**·(**2**·**3**) exhibits the characteristics of an Aviram–Ratner molecular rectifier[1] sandwiched by two electrodes. The observed rectification properties are reflected by the marked bias dependency of the STM contrast for heterocomplex **1**·(**2**·**3**), in which alternately brighter and darker areas appear with positive and negative sample bias voltages, respectively. Moreover, first-principles transport simulations reproduce the experimental results and reveal how the electronic rectification properties are developed in heterocomplex **1**·(**2**·**3**). Our study provides fundamental guidance toward the potential applications in molecular electronic devices with adjustable electronic functions using π-stacked systems as modular components.

DOI: 10.1021/jacs.5b00086
J. Am. Chem. Soc. 2015, 137, 5939–5947

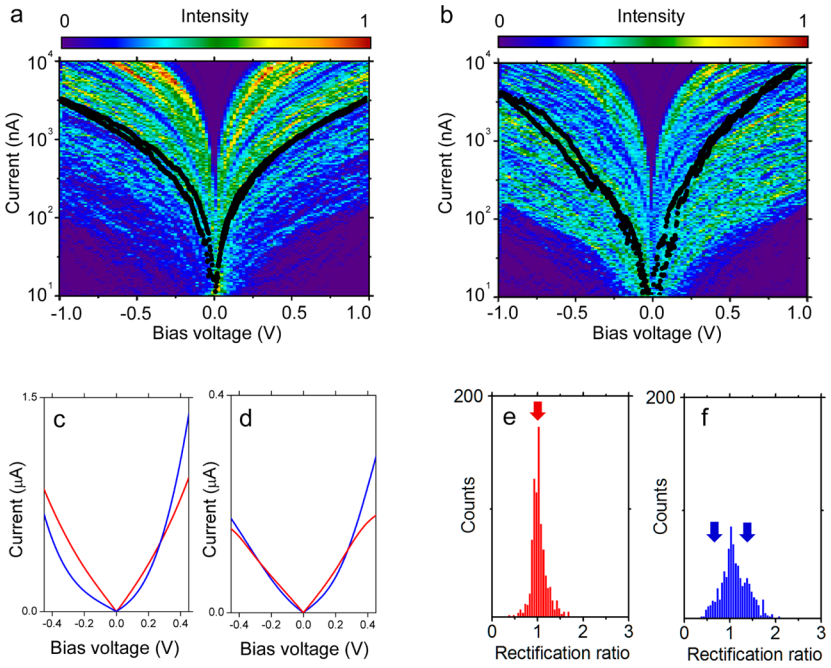

Figure 4. Current versus bias voltage characteristics (I–V) for the π-stacked complexes. (a,b) 2D histograms of the I–V curves for homocomplex **1**·(**3**·**3**) (a) and heterocomplex **1**·(**2**·**3**) (b), which are constructed from 500 I–V traces obtained under ambient conditions at room temperature. A linear X-bin-size of 0.02 V and a logarithmic Y-bin-size ($\Delta\log(I/\mathrm{nA})$) of 0.02 were used. Examples of I–V curves without and with rectification properties for the homo and hetero complexes are superimposed on the histograms (bold black lines). The histograms of (a) and (b) are characterized by large intensities in the current ranges of ca. 10^3–10^4 and 10^2–10^4 nA at ±1 V, respectively. (c,d) Examples of I–V curves without and with rectification properties for the homo (red) and hetero (blue) complexes. I–V curves within conductance windows of (c) $10^{-2}\ G_0 < G\ 10^{-1}\ G_0$ and (d) $10^{-3}\ G_0 < G < 10^{-2}\ G_0$ (at 1 V) are displayed. The bias polarity of the I–V curves was adjusted so that the forward bias direction corresponds to the positive bias voltage. (e,f) Histograms of the rectification ratio at the bias range at 0.4–0.5 V for the (e) homo and (f) hetero π-stacked complexes. The mean conductance values in the bias voltage range from +0.4 (−0.5) to +0.5 (−0.4) V were calculated for positive (negative) polarity. The rectification ratio is calculated as $R = \mathrm{mean}G_+/\mathrm{mean}G_-$, where R is the rectification ratio, and $\mathrm{mean}G_+$ and $\mathrm{mean}G_-$ are the mean conductance values in the negative and positive bias regions. Arrows indicated a sharp peak with a rectification factor of 1 for the homocomplex (blue). Beside a peak with a rectification factor of 1, broad distribution with rectification factors around 0.73 and 1.38 are indicated by arrows for the heterocomplex (red). For further details, see Supporting Information 3.

RESULTS AND DISCUSSION

Preparation and Electronic Characterization of π-Stacked Complexes on Au(111) Surface. Homocomplex **1**·(**3**·**3**) and heterocomplex **1**·(**2**·**3**) were deposited on a Au(111) surface. Isolated individual π-stacked complexes were characterized according to nanometer-sized bright protrusions in the STM images (Figure 2a–d). During repeated STM imaging, surface diffusion of the complexes was not apparent, which indicated substantial interactions between the π-stacked complexes and the Au surface.[32,33,36] Closer inspection of the STM contrasts revealed that the homo and hetero π-stacked complexes with the same physical height display distinct STM contrasts on the Au(111) surface. Cross-sectional profiles of each π-stacked complex demonstrate that homocomplex **1**·(**3**·**3**) is more conductive than heterocomplex **1**·(**2**·**3**) (see Supporting Information 1). The averaged STM contrast of homocomplex **1**·(**3**·**3**) was 1.2 times larger than that of heterocomplex **1**·(**2**·**3**). Note that the STM intensity of homocomplex **1**·(**3**·**3**) is almost constant (Figure 2a,c), while heterocomplex **1**·(**2**·**3**) exhibits significant variation in the STM contrast (Figure 2b,d). This variation in the STM contrast should be ascribed to two types of junction configurations, **1**·(**2**·**3**) and **1**·(**3**·**2**), on the Au(111) surface (Figure 2e,f, see Supporting Information 1 and 2). The bias dependence of the STM contrasts was investigated for the isolated homo and heterocomplexes on a Au(111) surface for a series of repeated STM imaging (Figures 2g,h). The STM contrast of homocomplex **1**·(**3**·**3**) was almost the same at positive and negative sample bias voltages (Figure 2g), but heterocomplex **1**·(**2**·**3**) gave brighter (conductive) and darker (less conductive) images at positive and negative sample bias voltages, respectively (Figure 2h, see Supporting Information 1). This bias dependence suggests rectification behavior for heterocomplex **1**·(**2**·**3**), of which the stacking orders, **2**·**3** and **3**·**2**, on the Au surface are distinctly different.

Conductance Measurements of π-Stacked Complexes with Two Au Electrode Contacts. Single π-stacked complexes were trapped between two Au electrodes, and the intrinsic electron-transport properties were measured using the STM-BJ technique.[6] The STM-Au-tip was repeatedly moved into and out of contact with a Au substrate in the presence of molecules. Two dimensional (2D) histograms of the conductance traces are presented in Figure 3a–c,e,f,h,i. STM-BJ experiments are performed both in water (Figure 3a–d) and under UHV (Figure 3e–j). The first identified data point at a threshold value was set to distance = 0 in 2D histograms to overlap all individual traces in 2D space. The threshold values were 1 G_0 for Figures 3a–c and S4a,b, 0.1 G_0 for Figure 3h,i, and 0.001 G_0 for Figure 3e,f. The large intensity at 1 G_0 in Figures 3a–c and S4a,b corresponds to the formation of a monatomic Au contact,[37,38] and the breakage of the atomic Au contact leads to the formation of nanosized Au electrodes. The π-stacked complexes then stochastically bridge the gap between

DOI: 10.1021/jacs.5b00086
J. Am. Chem. Soc. 2015, 137, 5939–5947

the electrodes to form π-stacked junctions.[6] The formation of the π-stacked junctions appeared at 10^{-3}–10^{-2} G_0 for both homocomplex **1**·(**3**·**3**) and heterocomplex **1**·(**2**·**3**) in the 2D histograms obtained in the higher conductance range (Figure 3b,c). These results reconfirm that the insulating empty cage becomes conductive with the inclusion of aromatics into the cage[32] (see inset, Figure 3a). However, in the lower conductance range below 10^{-3} G_0, the situation was different for the homo and hetero π-stacked junctions (Figure 3e,f). In the lower conductance below 10^{-3} G_0, current fluctuation possibly due to high affinity and sticking probability of the π-stacked complexes to Au electrodes in the liquid environment perturbs conductance measurement. Therefore, STM-BJ experiments were also performed in the diluted molecular condition under UHV. The homo π-stacked junction showed an exponential decay of conductance with an increase in the distance between the Au electrodes (Figure 3e). In contrast, the hetero π-stacked junction possessed a distinct junction configuration with a considerably lower conductance value at around 10^{-4} G_0 (Figure 3f). From the conductance traces in the 2D histograms, 1D conductance histograms for homocomplex **1**·(**3**·**3**) and heterocomplex **1**·(**2**·**3**) were constructed, as shown in Figure 3d,g. The histogram for the homocomplex has a single peak at 5×10^{-3} G_0 (Figure 3d), while that for the heterocomplex has two distinct peaks at 3×10^{-3} G_0 and 1×10^{-4} G_0 (Figure 3d,g). The two distinct conductance states for the hetero π-stacked complex **1**·(**2**·**3**) are attributed to the different junction configurations, **2**·**3** and **3**·**2**, along the electron-transport direction. To check the environmental effects of the molecular junctions[39−41] and robustness of the molecular conductance measured under liquid and UHV environments, STM-BJ experiments were further performed for the heterocomplex under UHV, in which background tunneling currents are strongly suppressed and two molecular conductance of $G_{\text{hetero\_1}}$ and $G_{\text{hetero\_2}}$ is reproduced (Figure 3h–j).

Current versus Bias Voltage Measurement. To directly capture the rectification properties of hetero π-stacked complex **1**·(**2**·**3**), current versus bias voltage (I–V) measurements were performed using the STM-BJ setup. In a similar manner to the conductance measurements (Figure 3), molecular junctions were prepared by repeatedly breaking an Au atomic contact under a fixed bias voltage of 0.02 V at a stretching rate of 40 nm/s and stochastically trapping a molecule into the gap between Au nanoelectrodes. In each breaking cycle, the electrode separation was fixed after breakage of the Au atomic contact and the bias voltage was swept from +0.02 to +1 V, then from +1 to −1 V and back to 0.02 V with an acquisition time of ca. 3 ms per sweep cycle (for further details, see Supporting Information 3). The 2D histograms of the I–V characteristics in Figure 4 are constructed from 500 I–V curves for the molecular junctions. For the STM-BJ experiment, orientation of the π-stacked complexes (i.e., stacking order of the D–D and D–A pairs for homo and hetero π-stacked complexes) along the electron transport direction was uncontrollable. Therefore, the rectification properties, if present, appear in both the positive and negative bias voltage regions. 2D histograms of the I–V curves for homocomplex **1**·(**3**·**3**) and heterocomplex **1**·(**2**·**3**) are shown in Figure 4a,b, respectively. The homocomplex is characterized by a high intensity in the narrow current range of 10^3–10^4 nA at a higher bias voltage of ±1 V (Figure 4a). The symmetric I–V curves at the positive and negative bias voltages reflect the unique junction configuration with a symmetric stacking order of **3**·**3** (see bold black lines representing an example of an I–V curve in Figure 4a). In contrast, the heterocomplex is characterized by a high intensity in the wide current range of 10^2–10^4 nA at ±1 V (Figure 4b). The wide distribution reflects the rectification properties and the variation in the junction configurations of the hetero π-stacked complex, which is in good agreement with the conductance measurements (Figure 3). The wide-ranged, asymmetric I–V curves at the positive and negative bias voltages reflect the distinct junction configurations of the heterocomplex (see bold black lines representing the I–V curve in Figure 4b). Examples of the I–V curves for homo and hetero π-stacked junctions are shown in Figures 4c,d. In the negative bias voltage region, the homo π-stacked junctions displays larger (Figure 4c) or similar (Figure 4d) current than that of the hetero π-stacked junction, while at the positive bias region, the current of the hetero π-stacked junction crosses over that of the homo π-stacked junction around +0.3 V, which is attributable to the effect of the rectification behavior for the hetero π-stacked junctions.

Statistical analysis of the I–V curves in Figure 4 reveals molecular-dependent rectification properties. The homo π-stacked complex indicated a sharp peak at a rectification ratio of 1 in the rectification histogram (Figure 4e), while the hetero π-stacked complex displayed broad distributions around rectification ratios of 0.73 (0.73 = 1/1.38) and 1.38 in addition to a peak at 1 in the rectification histogram (Figure 4f). The rectification ratio is calculated as $R = \text{mean}G_+/\text{mean}G_-$, where R is the rectification ratio, and $\text{mean}G_+$ and $\text{mean}G_-$ are the mean conductance values in the positive and negative bias regions (see the caption in Figure 4). In earlier studies averaged rectification ratios of 2.5[23] and 1.7[25] have been reported in statistical analysis for 50 and ca. 5000 I–V curves, respectively. In these studies, the rectification ratio for each I–V curve varied within the range of 1–5[23] and 1–3.5.[25] We obtained a similar rectification ratio of 1 as a peak structure in the rectification histogram (Figure 4f). We suspect without stringent evidence that the rectification ratio of 1 could come from (i) ill-defined metal-molecule contact configurations during the repeated I–V measurements within the high bias range of ±1.0 V and (ii) annihilation of the rectification property due to pairwise formation of molecular junctions with alternative molecular orientation along a charge transport direction. The two rectification factors of 0.73 and 1.38 found in the present study could correspond to two distinct orientations (i.e., forward and backward orientations) of the heterocomplex along the charge transport direction. The tail of the distribution around 1.38 for the hetero π-stacked junctions indicates a rectification ratio of up to 2. The statistical approach provides experimental evidence for the unique rectification properties of the hetero π-stacked junctions at the higher bias range.[42] Earlier studies on single molecular diode have demonstrated rectification ratios of 1.4–10,[21] 4.5–9,[22] 1–5,[23] and 1.5–11[24] for π-conjugated molecular junctions with (π-donor)–(σ-spacer)–(π-acceptor) systems. A rectification histogram has been presented in a pioneering study, where statistical analysis of the rectification ratio was not the main focus.[21] A recent study on single molecular diode with asymmetric metal-molecule contacts system has performed statistical analysis of I–V curves, in which measured I–V characteristics were classified into three groups with (i) rectification ratio > 1 (ii) rectification ratio < 1 and (iii) rectification ratio = 1.[25] Sorted I–V curves are then averaged to make a single I–V curve, in

DOI: 10.1021/jacs.5b00086
J. Am. Chem. Soc. 2015, 137, 5939–5947

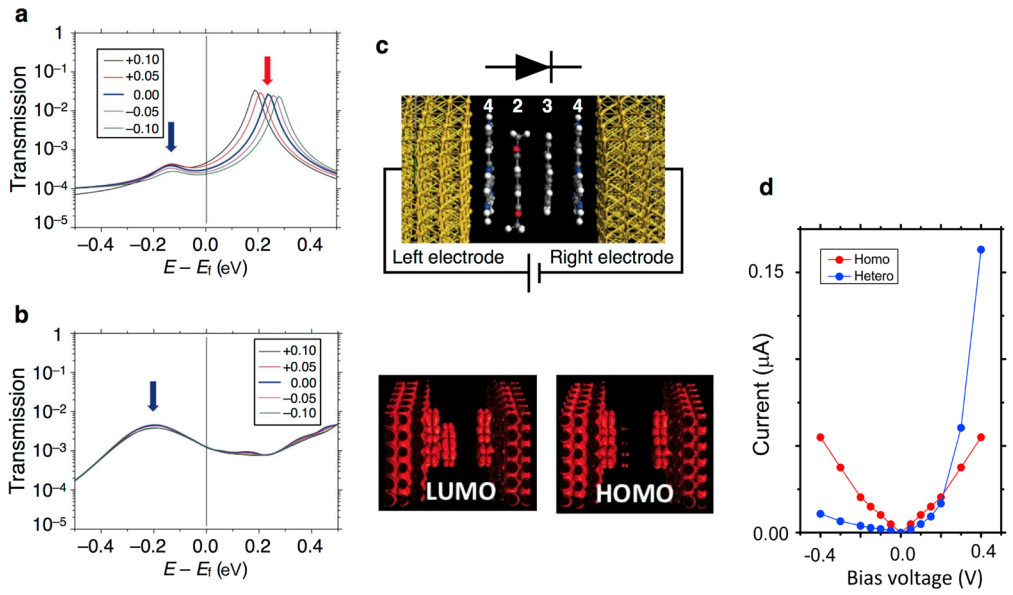

Figure 5. First-principles simulation of transport properties. (a,b) Calculated gap-corrected transmission functions of hetero π-stack model **4**·(**2**·**3**)·**4** (a) and homo π-stack model **4**·(**3**·**3**)·**4** (b) sandwiched between Au electrodes. The magnitudes of the applied bias voltages between the left and right electrodes are shown in the inset. (c) Schematic illustration of the hetero π-stacked **4**·(**2**·**3**)·**4** junction model for transmission calculations. The bias polarity in the illustration corresponds to a positive bias application, and the rectification direction is also indicated at the top. The two panels at the bottom side are the local density of states corresponding to the HOMO and LUMO peaks of the hetero π-stacked junction. Gray, white, red, and blue spheres represent C, H, O, and N atoms. (d) Calculated electronic current under applied bias voltage in the homo (red) and hetero (blue) π-stacked junctions.

which averaged rectification ratio of 1.7 was found. Variation in rectification ratio in a single $I-V$ curve was reported to be 1−3.8.[25] The rectification ratio of 1.38 (1/0.73) found in the histogram is comparable to the averaged rectification ratio of 1.7 found for the averaged $I-V$ curve in the previous study.[25] The averaged rectification ratio of 1.38 in Figure 4f is smaller than the expected rectification ratio for the conductance measurement, i.e., $(3 \times 10^{-3}\ G_0)/(1 \times 10^{-4}\ G_0) > 10$ in Figure 3d,g,j. We attribute this gap in the rectification ratio to difference in preferential junction-structures formed in the conductance measurement at the constant bias voltage below 0.15 V and in the $I-V$ measurement under repeat bias voltage sweeps up to the high bias of 1.0 V. It should be noted that, along with the effort for statistical analysis of rectification behavior, much effort has been devoted to controlling the orientation of the single molecular diode along the charge transport direction. Based on step by step formation of metal-molecule contacts, the molecular orientation has been successfully controlled to clarify the diode effect.[22,23]

Next we comment on electronic conductivity for the single molecular diode of the π-stacked system by comparing the conductivity with those found for single molecular diodes in the previous studies.[21−25] It has been demonstrated that current values at the forward bias (at 1 V) are (i) 1 nA[21] for phenylethynyl-perfluorophenylethynyl system, (ii) 0.03,[22] 100,[23] and 10 nA[24] for a same dipyrimidinyl-diphenyl system, and (iii) 600−700 nA[25] for diphenylethene with asymmetric metal-molecule contacts system. In the present system, the current is within the current range of 10^2-10^4 nA. Average current among 1000 of $I-V$ curves is 1.6 μA at 1 V for the hetero π-stacked junctions, while average current for the homo π-stacked junctions is 2.6 μA at 1 V. The conductivity of the π-stacked diode is higher than those of the (π-donor)−(σ-spacer)−(π-acceptor) systems with "Au-thiolate" metal-molecule contacts and is comparable with that of the diphenylethene with asymmetric metal-molecule contacts of "Au-methylsulfide" and covalent "Au-C" contacts-system. In contrast to the resistive "Au-thiolate" binding in the earlier studies, the conductive direct metal-π binding[21] used in this study brings the increased electronic transparency into the single molecular diode.

First-Principles Simulation of Transport Properties. To probe the physics behind the observed rectification behavior, first-principles electron transport calculations were performed for the homo and hetero π-stacked junctions using the nonequilibrium Green's function (NEGF) method[43] combined with density functional theory (DFT) implemented with the ATK program.[44−46] To reduce the calculation cost, cage **1** was replaced with the top and bottom aromatic panels **4** (Figure 1), and hence, π-stacked systems **4**·(**3**·**3**)·**4** and **4**·(**2**·**3**)·**4** were used as simple models in the calculations for homostack **1**·(**3**·**3**) and heterostack **1**·(**2**·**3**), respectively.[32] In this study, the NEGF-DFT transmission functions with corrected energy gap were calculated and analyzed (see Supporting Information 4 for computational details).

Figure 5a,b shows the gap-corrected transmission curves for hetero π-stacked **4**·(**2**·**3**)·**4** and homo π-stacked **4**·(**3**·**3**)·**4** sandwiched between Au electrodes, respectively. The hetero π-stacked junction, as illustrated in Figure 5c, exhibited a rectifying response in the $I-V$ curve (Figure 5d), whereas the homo π-stacked junction did not, which indicates a qualitative agreement to the experimental observations (Figure 4c,d). The rectifying response for the hetero π-stacked junction originates from the unique response of the transmission peaks with respect to the applied bias voltages; the transmission peak of LUMO (red arrow) of the hetero π-stacked junction shows upward/downward shift with respect to the negative/positive bias applications, but the peaks of HOMOs (blue arrows) of the homo and hetero π-stacked junctions are almost insensitive against the applied bias voltages. When we apply the bias

DOI: 10.1021/jacs.5b00086
J. Am. Chem. Soc. 2015, 137, 5939−5947

voltage of +2X or −2X volt, the integral of the transmission function in the range from −X to +X eV is proportional to the current. The range of the integral, −X to +X eV, is called the bias window, and the bias window is exactly the same in both bias applications of +2X and −2X volt. Since the transmission function of the homo π-stacked junction is not changed against the bias applications, the integrals of the transmission function at the bias of +2X and −2X volt are the same, resulting in the same magnitude of current (i.e., no rectifying response). On the other hand, in the hetero π-stacked junction, the large LUMO peak is approaching toward the Fermi level in the positive bias applications (e.g., +2X volt) and moving toward higher energy in the negative bias applications (e.g., −2X volt). That is, the shape of transmission functions are significantly different between the positive and negative bias applications in the hetero π-stacked junction, and the integral of the transmission function at the positive bias applications significantly includes the positive contribution of the large LUMO peak. That is why the larger current is obtained at the positive bias applications, leading to the clear rectifying response in the hetero π-stacked junction.

The origins of the LUMO level shift and HOMO level silence with respect to bias applications in the π-stacked junctions are understood by looking at the local density of states. The local density of states at 0.2 eV above the Fermi level (i.e., the large sensitive peak for the hetero π-stacked junction) indicates strong hybridization between the left electrode, the neighboring triazine panel **4**, and π-acceptor **2** (see LUMO in Figure 5c). This asymmetric spatial distribution of the LUMO channel along the electron transport direction is apparent under applied bias conditions (not shown here). Thus, when the bias voltage is applied to the hetero π-stacked junction, the orbital level mainly follows the Fermi level of the left Au electrode, which corresponds to the observed shift of the transmission peak in Figure 5a. On the other hand, the local density of states at 0.2 eV below the Fermi level (i.e., the insensitive peaks in both the hetero and homo π-stacked junctions) corresponds to equivalent delocalization of the orbital to triazine panel **4** on the left and the right Au electrode (see HOMO in Figure 5c). Thus, when a positive/negative bias is applied to the left/right electrode, the shift down of the HOMO level by the left electrode is almost perfectly canceled by the shift-up of the HOMO level by the right Au electrode, which leads to the insensitive transmission peak with respect to the bias voltage. In this way, the asymmetric contribution of the transmission LUMO channel results in bias voltage-dependent transport.

The transport calculations suggest that (i) the π-stacked junctions exhibit distinct electronic conductance (i.e., the homo π-stacked junction is more conductive than the hetero π-stacked junction) that is dependent on the π-stacked content and (ii) rectification behavior is apparent for the hetero π-stacked junction with a rectification ratio of ca. 2.4 at the lower bias voltage of ±0.1 V but is absent for the homo π-stacked junction. The resultant transmission channels of the π-stacked complexes sandwiched between two Au electrodes appear close to the Au Fermi energy in the energy range of ±0.3 eV, which leads to higher electronic transparency and significant responsivity of the transmission channel with respect to the bias voltage applied between the Au electrodes. Combined experimental and theoretical characterization of the electronic properties for cage **1** accommodating π-stacked molecules revealed that the content and stacking order of the π-stacked molecules has a considerable impact on the electronic functionality.

Based on STM imaging, STM-BJ experiments, and first-principles transport calculations, the electronic properties of self-assembled coordination cage **1** containing homo and hetero π-stacked molecules have been revealed by fixing the cage complex between two Au electrodes. The homo π-stacked junction displays highly conductive character with a conductance of 5×10^{-3} G_0 and acts as a π-stacked wire (resistor) that conducts electronic charge. The hetero π-stacked junctions exhibit electronic rectification properties with conductances of 3×10^{-3} G_0 and 1×10^{-4} G_0 for the forward and backward bias directions, respectively, in the conductance measurements at a fixed bias voltage. I−V characterization of the hetero π-stacked junctions revealed unique rectification ratio of 1.38−2. The rectification direction can be controlled by the stacking order of π-conjugated molecules in the cage.

Finally we discuss the limitation and issue of our system and the direction of future research. In the present study orientation of π-stacked diode, i.e., stacking order of the aromatics in the cage against a charge transport direction is hardly controlled. DFT energetic investigation for the **1**·(**2**·**3**) and **1**·(**3**·**2**) species on the Au(111) revealed that **1**·(**3**·**2**)/Au(111) configuration is ∼0.2 eV more stable than that of **1**·(**2**·**3**)/Au(111). We are looking for other hetero π-stacked systems where energy differences between two molecular orientation on Au(111) become larger. We believe that molecular orientations of hetero complexes on Au(111) can be controlled if we could take advantage of energetic difference between the two orientations. Along with the control over the molecular orientation, design of modular aromatics in the cage is required in future studies to improve the devise performance such as conductivity, rectification behavior in molecular diode, etc.

■ CONCLUSION

Many studies to date have been conducted on the rectification properties of single-molecule junctions,[21−25,47−49] in which π-conjugated molecules with (π-donor)−(σ-spacer)−(π-acceptor) systems are frequently employed as an Aviram−Ratner model[1] and bound to two Au electrodes through terminal functional groups. However, the present study is distinct from the previous studies in that π-stacked complexes without covalent linkers are directly bound to the Au electrodes through their own π-conjugated planes[32,33,36] and that electron transport primarily occurs in a direction perpendicular to the π planes. Molecular self-assembly provides discrete π-stacked systems within the cage in solution, which enables elucidating the electron-transport properties and paves the way for the development of molecular electronic devices with tunable electronic functions.

■ METHODS

Sample Preparation and Deposition of Molecules. Cage **1**, homocomplex **1**·(**3**·**3**), and heterocomplex **1**·(**2**·**3**) were prepared using previously reported procedures.[35] The Au(111) substrates were prepared via the thermal evaporation of Au onto mica. The Au tips were prepared by electrochemical etching of Au wires in 12 M hydrochloric acid. For the ambient STM imaging and UHV-STM-BJ experiments, sample molecules were deposited by immersion of the substrate into the corresponding 0.05 mM aqueous solutions for several minutes. After deposition, the substrates were dried in an air flow.

STM Characterization and STM-BJ Measurement. STM imaging was performed under ambient conditions at room temper-

DOI: 10.1021/jacs.5b00086
J. Am. Chem. Soc. 2015, 137, 5939−5947

ature using a commercially available STM system (Digital Instruments Nanoscope III). STM-BJ experiments were performed in 0.5 mM molecular aqueous solutions and under UHV conditions using commercially available STMs (Molecular Imaging PicoScan and Jeol JSPM4500S). For the STM-BJ experiments, the tip was coated with Apiezon wax using a standard procedure to prevent a large electrochemical leakage current in the aqueous solutions, while a bare Au tip was used for ambient STM imaging and UHV-STM-BJ experiments (base pressure of 5×10^{-8} Pa). In the STM-BJ experiments, molecular junctions were typically formed by repeated formation and breaking of a Au point contact in the presence of the molecules. During the cycles, the molecules stochastically bridge the gap between two electrodes of the Au(111) substrate and Au tip. The details for this procedure are described elsewhere.[32,33,50]

Current versus Bias Voltage Measurement. Current versus bias voltage measurements were performed under ambient conditions at room temperature using the same experimental STM-BJ-setup in solution. During the breaking process of the Au atomic contact at the fixed bias voltage of 0.02 V, the conductance jumps from 1−3 G_0 to below 1 G_0 immediately after the breakage of the Au contact. The separation of the electrodes is then fixed, and the bias voltage is swept from +0.02 to +1 V, then from +1 to −1 V, and back to +0.02 V with an acquisition time of ca. 3 ms per sweep (see Supporting Information 3).

DFT Calculations. Electron transport calculations based on DFT and NEGF were conducted to determine the key to the rectification response of the π-stack junction. The rectifying properties are sensitive to the orbital levels of the sandwiched molecule (i.e., HOMO, LUMO); therefore, the HOMO−LUMO gap of the Au_{19}−[hetero π-stacked **4**·(**2**·**3**)·**4**]−Au_{19} extended molecular system was first calculated using hybrid DFT at the B3LYP[51,52] level of theory with CEP-31G basis set[53] in Gaussian09,[54] and the transmission functions were reconstructed using the HOMO−LUMO gap. Details of the computational conditions used for the transmission calculations and gap correction are described in Supporting Information 4.

■ ASSOCIATED CONTENT

Supporting Information

Experimental details on STM electronic characterization, STM-BJ conductance measurement and STM-BJ current versus bias voltage measurement, DFT calculations. The Supporting Information is available free of charge on the ACS Publications website at DOI: 10.1021/jacs.5b00086.

■ AUTHOR INFORMATION

Corresponding Authors

*fujii.s.af@m.titech.ac.jp
*tada.t.ae@m.titech.ac.jp
*mfujita@appchem.t.u-tokyo.ac.jp
*kiguti@chem.titech.ac.jp

Notes

The authors declare no competing financial interest.

■ ACKNOWLEDGMENTS

This research was supported in part by the Ministry of Education, Culture, Sports, Science and Technology (MEXT) of Japan (Grant-in-Aid for Scientific Research: 24245027 to M.K., no. 25708008 to T.M., and no. 24000009 to M.F.). T.T. acknowledges the Element Strategy Initiative to Form Core Research Center of MEXT, Japan.

■ REFERENCES

(1) Aviram, A.; Ratner, M. A. *Chem. Phys. Lett.* **1974**, *29*, 277.
(2) Joachim, C.; Ratner, M. A. *Proc. Natl. Acad. Sci. U.S.A.* **2005**, *102*, 8801.
(3) van Ruitenbeek, J. M.; Alvarez, A.; Piñeyro, I.; Grahmann, C.; Joyez, P.; Devoret, M. H.; Esteve, D.; Urbina, C. *Rev. Sci. Instrum.* **1996**, *67*, 108.
(4) Smit, R. H. M.; Noat, Y.; Untiedt, C.; Lang, N. D.; van Hemert, M. C.; van Ruitenbeek, J. M. *Nature* **2002**, *419*, 906.
(5) Reed, M. A.; Zhou, C.; Muller, C. J.; Burgin, T. P.; Tour, J. M. *Science* **1997**, *278*, 252.
(6) Xu, B. Q.; Tao, N. J. *Science* **2003**, *301*, 1221.
(7) Tao, N. J. *Nat. Nanotechnol.* **2006**, *1*, 173.
(8) Lindsay, S. M.; Ratner, M. A. *Adv. Mater.* **2007**, *19*, 23.
(9) Tsutsui, M.; Taniguchi, M. *Sensors* **2012**, *12*, 7259.
(10) Aradhya, S. V.; Venkataraman, L. *Nat. Nanotechnol.* **2013**, *8*, 399.
(11) Kiguchi, M.; Kaneko, S. *Phys. Chem. Chem. Phys.* **2013**, *15*, 2253.
(12) Donhauser, Z. J.; Mantooth, B. A.; Kelly, K. F.; Bumm, L. A.; Monnell, J. D.; Stapleton, J. J.; Price, D. W.; Rawlett, A. M.; Allara, D. L.; Tour, J. M.; Weiss, P. S. *Science* **2001**, *292*, 2303.
(13) Blum, A. S.; Kushmerick, J. G.; Long, D. P.; Patterson, C. H.; Yang, J. C.; Henderson, J. C.; Yao, Y.; Tour, J. M.; Shashidhar, R.; Ratna, B. R. *Nat. Mater.* **2005**, *4*, 167.
(14) Lörtscher, E.; Ciszek, J. W.; Tour, J.; Riel, H. *Small* **2006**, *2*, 973.
(15) Liljeroth, P.; Repp, J.; Meyer, G. *Science* **2007**, *317*, 1203.
(16) Quek, S. Y.; Kamenetska, M.; Steigerwald, M. L.; Choi, H. J.; Louie, S. G.; Hybertsen, M. S.; Neaton, J. B.; Venkataraman, L. *Nat. Nanotechnol.* **2009**, *4*, 230.
(17) Kiguchi, M.; Ohto, T.; Fujii, S.; Sugiyasu, K.; Nakajima, S.; Takeuchi, M.; Nakamura, H. *J. Am. Chem. Soc.* **2014**, *136*, 7327.
(18) Dulić, D.; van der Molen, S. J.; Kudernac, T.; Jonkman, H. T.; de Jong, J. J. D.; Bowden, T. N.; van Esch, J.; Feringa, B. L.; van Wees, B. J. *Phys. Rev. Lett.* **2003**, *91*, 207402.
(19) Kim, Y.; Hellmuth, T. J.; Sysoiev, D.; Pauly, F.; Pietsch, T.; Wolf, J.; Erbe, A.; Huhn, T.; Groth, U.; Steiner, U. E.; Scheer, E. *Nano Lett.* **2012**, *12*, 3736.
(20) Meng, F.; Hervault, Y.-M.; Shao, Q.; Hu, B.; Norel, L.; Rigaut, S.; Chen, X. *Nat. Commun.* **2014**, *5*, 3023.
(21) Elbing, M.; Ochs, R.; Koentopp, M.; Fischer, M.; von Hänisch, C.; Weigend, F.; Evers, F.; Weber, H. B.; Mayor, M. *Proc. Natl. Acad. Sci. U.S.A.* **2005**, *102*, 8815.
(22) Morales, G. M.; Jiang, P.; Yuan, S.; Lee, Y.; Sanchez, A.; You, W.; Yu, L. *J. Am. Chem. Soc.* **2005**, *127*, 10456.
(23) Díez-Pérez, I.; Hihath, J.; Lee, Y.; Yu, L.; Adamska, L.; Kozhushner, M. A.; Oleynik, I. I.; Tao, N. *Nat. Chem.* **2009**, *1*, 635.
(24) Lörtscher, E.; Gotsmann, B.; Lee, Y.; Yu, L.; Rettner, C.; Riel, H. *ACS Nano* **2012**, *6*, 4931.
(25) Batra, A.; Darancet, P.; Chen, Q.; Meisner, J. S.; Widawsky, J. R.; Neaton, J. B.; Nuckolls, C.; Venkataraman, L. *Nano Lett.* **2013**, *13*, 6233.
(26) Xu, B.; Xiao, X.; Yang, X.; Zang, L.; Tao, N. *J. Am. Chem. Soc.* **2005**, *127*, 2386.
(27) Pobelov, I. V.; Li, Z.; Wandlowski, T. *J. Am. Chem. Soc.* **2008**, *130*, 16045.
(28) Capozzi, B.; Chen, Q.; Darancet, P.; Kotiuga, M.; Buzzeo, M.; Neaton, J. B.; Nuckolls, C.; Venkataraman, L. *Nano Lett.* **2014**, *14*, 1400.
(29) Chen, F.; He, J.; Nuckolls, C.; Roberts, T.; Klare, J. E.; Lindsay, S. *Nano Lett.* **2005**, *5*, 503.
(30) Park, J.; Pasupathy, A. N.; Goldsmith, J. I.; Chang, C.; Yaish, Y.; Petta, J. R.; Rinkoski, M.; Sethna, J. P.; Abruna, H. D.; McEuen, P. L.; Ralph, D. C. *Nature* **2002**, *417*, 722.
(31) Song, H.; Kim, Y.; Jang, Y. H.; Jeong, H.; Reed, M. A.; Lee, T. *Nature* **2009**, *462*, 1039.
(32) Kiguchi, M.; Takahashi, T.; Takahashi, Y.; Yamauchi, Y.; Murase, T.; Fujita, M.; Tada, T.; Watanabe, S. *Angew. Chem., Int. Ed.* **2011**, *50*, 5708.
(33) Kiguchi, M.; Inatomi, J.; Takahashi, Y.; Tanaka, R.; Osuga, T.; Murase, T.; Fujita, M.; Tada, T.; Watanabe, S. *Angew. Chem., Int. Ed.* **2013**, *52*, 6202.
(34) Klosterman, J. K.; Yamauchi, Y.; Fujita, M. *Chem. Soc. Rev.* **2009**, *38*, 1714.

DOI: 10.1021/jacs.5b00086
J. Am. Chem. Soc. 2015, 137, 5939−5947

(35) Murase, T.; Otsuka, K.; Fujita, M. *J. Am. Chem. Soc.* **2010**, *132*, 7864.
(36) Schneebeli, S. T.; Kamenetska, M.; Cheng, Z.; Skouta, R.; Friesner, R. A.; Venkataraman, L.; Breslow, R. *J. Am. Chem. Soc.* **2011**, *133*, 2136.
(37) Ohnishi, H.; Kondo, Y.; Takayanagi, K. *Nature* **1998**, *395*, 780.
(38) Agraït, N.; Yeyati, A. L.; van Ruitenbeek, J. M. *Phys. Rep.* **2003**, *377*, 81.
(39) French, W. R.; Iacovella, C. R.; Cummings, P. T. *ACS Nano* **2012**, *6*, 2779.
(40) Fatemi, V.; Kamenetska, M.; Neaton, J. B.; Venkataraman, L. *Nano Lett.* **2011**, *11*, 1988.
(41) Nakashima, S.; Takahashi, Y.; Kiguchi, M.; Beilstein, J. *Nanotechnology* **2011**, *2*, 755.
(42) Although statistical analysis of the rectification ratio at the lower bias rage of 0.1−0.2V (not shown here) exhibited rectification ratios up to a factor of ∼8, fluctuation of the current and widely spreaded ratios at the lower bias voltage prevents statistical analysis of the rectification ratio, which is due to our experimental setup with low gain-current amplifier.
(43) Datta, S. *Electronic transport in mesoscopic systems*; Cambridge University Press: Cambridge, U.K., 1995.
(44) Brandbyge, M.; Mozos, J.-K.; Ordejón, P.; Taylor, J.; Stokbro, K. *Phys. Rev. B* **2002**, *65*, 165401.
(45) Soler, J. M.; Artacho, E.; Gale, J. D.; Garcia, A.; Junquera, J.; Ordejon, P.; Sanchez-Portal, D. *J. Phys.: Condens. Matter* **2002**, *14*, 2745.
(46) *ATK Manual ATK version 12.8.0*; QuantumWise A/S: Copenhagen, Denmark; http://www.quantumwise.com.
(47) Nakamura, H.; Asai, Y.; Hihath, J.; Bruot, C.; Tao, N. *J. Phys. Chem. C* **2011**, *115*, 19931.
(48) Tsuji, Y.; Yoshizawa, K. *J. Phys. Chem. C* **2012**, *116*, 26625.
(49) Müllen, K.; Rabe, J. P. *Acc. Chem. Res.* **2008**, *41*, 511.
(50) Fujii, S.; Akiba, U.; Fujihira, M. *Chem. Lett.* **2008**, *37*, 408.
(51) Becke, A. D. *J. Chem. Phys.* **1993**, *98*, 5648.
(52) Lee, C.; Yang, W.; Parr, R. G. *Phys. Rev. B* **1988**, *37*, 785.
(53) Stevens, W. J.; Basch, H.; Krauss, M. *J. Chem. Phys.* **1984**, *81*, 602.
(54) Frisch, M. J.; Trucks, G. W.; Schlegel, H. B.; Scuseria, G. E.; Robb, M. A.; Cheeseman, J. R.; Scalmani, G.; Barone, V.; Mennucci, B.; Petersson, G. A.; Nakatsuji, H.; Caricato, M.; Li, X.; Hratchian, H. P.; Izmaylov, A. F.; Bloino, J.; Zheng, G.; Sonnenberg, J. L.; Hada, M.; Ehara, M.; Toyota, K.; Fukuda, R.; Hasegawa, J.; Ishida, M.; Nakajima, T.; Honda, Y.; Kitao, O.; Nakai, H.; Vreven, T.; Montgomery, J. A., Jr.; Peralta, J. E.; Ogliaro, F.; Bearpark, M.; Heyd, J. J.; Brothers, E.; Kudin, K. N.; Staroverov, V. N.; Kobayashi, R.; Normand, J.; Raghavachari, K.; Rendell, A.; Burant, J. C.; Iyengar, S. S.; Tomasi, J.; Cossi, M.; Rega, N.; Millam, J. M.; Klene, M.; Knox, J. E.; Cross, J. B.; Bakken, V.; Adamo, C.; Jaramillo, J.; Gomperts, R.; Stratmann, R. E.; Yazyev, O.; Austin, A. J.; Cammi, R.; Pomelli, C.; Ochterski, J. W.; Martin, R. L.; Morokuma, K.; Zakrzewski, V. G.; Voth, G. A.; Salvador, P.; Dannenberg, J. J.; Dapprich, S.; Daniels, A. D.; Farkas, Ö.; Foresman, J. B.; Ortiz, J. V.; Cioslowski, J.; Fox, D. J. *Gaussian 09*, Revision C.01; Gaussian, Inc.: Wallingford, CT, 2010.

DOI: 10.1021/jacs.5b00086
J. Am. Chem. Soc. 2015, 137, 5939−5947